Journal of Power Sources 219 (2012) 163–171

Contents lists available at SciVerse ScienceDirect

Journal of Power Sources

journal homepage: www.elsevier.com/locate/jpowsour

Synergy among transition element, nitrogen, and carbon for oxygen reduction reaction in alkaline medium

Zhou Peng Li [a], Zi Xuan Liu [a], Kun Ning Zhu [a], Zhuo Li [a], Bin Hong Liu [b,*]

[a] Department of Chemical and Biological Engineering, Zhejiang University, Hangzhou 310027, PR China
[b] Department of Materials Science and Engineering, Zhejiang University, Hangzhou 310027, PR China

HIGHLIGHTS

- Cooperative interaction among Co, N and C is the key to enhance oxygen reduction reaction (ORR).
- Individual interactions between C and N, C and Co, Co and N have little effect on the ORR enhancement.
- Doping effect on ORR enhancement is dependent on the natures of the transition element and anion.

GRAPHICAL ABSTRACT

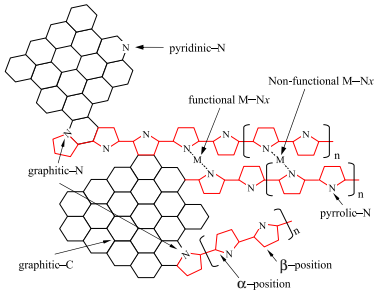

ARTICLE INFO

Article history:
Received 13 May 2012
Received in revised form
12 July 2012
Accepted 13 July 2012
Available online 21 July 2012

Keywords:
Pt alternative catalyst
Oxygen reduction reaction
Synergy
Polypyrrole modification
Transition element doping
Hydrothermal treatment

ABSTRACT

A series of M-doped polypyrrole (PPy)-modified BP2000 catalysts (M = Mn, Fe, Co, Ni, and Cu) are synthesized using the hydrothermal method. The synergy among a transition element, nitrogen, and carbon for oxygen reduction reaction (ORR) in alkaline medium is discussed based on the physical characterization and electrochemical analyses of the Co-doped PPy-modified BP2000. PPy is found to adhere carbon black particles together to form a porous 3D network during the PPy modification on BP2000. PPy reconfiguration occurs during the hydrothermal treatment process. The individual interactions between BP and PPy, BP and Co, and Co and PPy exhibit insignificant effects on the enhancement of ORR. The cooperative interaction among Co, N, and C plays a very important role in the enhancement of ORR. The doping effect of transition-metal salt on ORR enhancement depends on the nature of the transition element and the corresponding anion.

1. Introduction

The performance of a fuel cell or air battery is highly dependent on the rate of oxygen reduction reaction (ORR). Platinum is an excellent catalyst for ORR. However, the scarcity and high catalyst cost of Pt are big problems in fuel cell and air battery development. Thus, the search for Pt alternative catalysts for ORR has become one of the more important tasks in electrochemistry.

ORR is a complicated condition-sensitive multi-step reaction because the ORR pathway depends on the adsorption configuration of molecular oxygen and the interaction between molecular oxygen and catalytic sites [1,2]. Oxygen adsorption configuration depends on the crystallographic structure of the catalyst (geometrical effect) and the binding energy (chemical effect) between oxygen and catalytic sites.

In general, carbon exhibits poor electrocatalytic activity to ORR. However, carbon materials become reactive to oxygen molecular

* Corresponding author. Tel./fax: +86 571 87951770.
E-mail address: liubh@zju.edu.cn (B.H. Liu).

0378-7753/$ – see front matter © 2012 Elsevier B.V. All rights reserved.
http://dx.doi.org/10.1016/j.jpowsour.2012.07.041

when free radicals (with unpaired electrons) are formed on carbon surfaces [3]. Free radicals can be created by breaking the surface bonds of =C–H, C–O at a high temperature of 900 °C in vacuum. Furthermore, when carbon materials are doped with nitrogen, the formed N-doped carbons have fairly good electrocatalytic activity to oxygen reduction [4,5] because the created pyridinic-N and graphitic-N catalyze ORR [6, 7]. Pyridinic-N (–C=N–C) and graphitic-N represent the nitrogen atom bonded to two carbon atoms at the edges of graphite planes and the three carbon atoms within a graphite (basal) plane, respectively. Nitrogen donates an electron from its lone electron pair to the π-conjugated bond system, imparting Lewis basicity to the carbon [8] and enabling the carbon to adsorb molecular oxygen and transfer this electron to molecular oxygen to form intermediates, such as OH^-, O_2^-, and HO_2^-. These intermediates are very important to ORR [9,10].

Nitrogen plays an important role in ORR on N-doped carbons and organometallic compounds. Many nitrogen-containing organometallic compounds have comparable electrocatalytic activities to Pt [11]. M–N*x* sites in transition-metal macrocycles (e.g., tetramethoxy tetraphenyl porphyrin, phthalocyanine, tetraphenyl porphyrins, and tetraazaanulene) or in transition-metal macrocycle composites (e.g., polypyrrole and polyaniline) function as electrocatalytic sites for ORR, where M represents a transition-metal, such as Fe, Co, Ni, Mn, and Cu. Carbon-supported transition-metal compounds (e.g., Co/N/C and Fe/N/C) also exhibit fairly good electroactivity to ORR [12–14]. Polypyrrole (PPy) modification can significantly improve the ORR kinetics on carbon-supported $Co(OH)_2$ catalysts [15–17]. Several electrocatalytic sites may coexist in the catalysts mentioned above. Many studies [18–22] claimed that the Co–N*x* and –C=N–C sites on carbon-supported catalysts are the catalytic sites for ORR. However, the fundamentals of nitrogen- and transition-metal-doping effects on ORR enhancement are unclear. Less attention has been paid to the interaction between M–N*x* and the carbon from the catalyst support.

In this study, a series of catalysts with different compositions is synthesized using the hydrothermal method to investigate the interactions among catalyst components. The catalytic sites and the synergy among a transition element, nitrogen (from PPy), and carbon (from catalyst support) are discussed based on the results of physical characterization and electrochemical analysis.

2. Experimental details

2.1. Catalyst synthesis

The procedure for the preparation of PPy-modified BP2000 (PPy/BP) was described in a previous study [15]. Carbon dispersion was prepared by adding 10 g of carbon powder (BP2000) and 2.5 mL of glacial acetic acid to 150 mL of de-ionized water after stirring for 20 min under room temperature. Then, 2 g of pyrrole and 10 mL of H_2O_2 solution (10 wt.%) were added to the carbon dispersion to load PPy on the surfaces of the BP2000 powders. The PPy/BP sample was obtained after stirring for 3 h in the dark, filtering, washing, and finally, drying at 90 °C under vacuum for 10 h. The loading of PPy on the carbon was approximately 17 wt.%.

M-doped catalysts (M = Mn, Fe, Co, Ni, and Cu) were prepared using the hydrothermal method. Then, 0.7 g of the PPy/BP was added to a vessel containing 100 mL of transition-metal salt solution (12 mmol L^{-1}). After ultrasonic mixing for 20 min, the vessel was sealed and placed into an incubator for 12 h at 60 °C. The M-doped PPy-modified BP2000 (M-doped PPy/BP) was then obtained after filtrating and washing repeatedly with warm de-ionized water and after drying at 90 °C under vacuum for 12 h.

2.2. Structural characterization and elemental identification

The microstructure and morphology of the synthesized catalysts were characterized via X-ray diffraction (XRD) using a Rigaku-D/MAX-2550PC diffractometer with Cu Kα radiation ($\lambda = 1.5406$ Å) and scanning electron microscopy (SEM), respectively. The chemical valence states of Co, N, O, and C were investigated through X-ray photoemission spectroscopy (XPS) using a PHI-5000C ESCA system (Perkin Elmer Inc., USA) with Mg Kα radiation ($h\nu = 1253.6$ eV). All spectra were referenced to the C ls level at 284.6 eV to correct the peak shift that occurred because of the charge accumulation on the sample. Data analysis was performed using the RBD AugerScan 3.21 software by RBD Enterprises. For convenience in analysis, all spectra were normalized based on the relative surface content of each constituent. The Fourier transform infrared (FTIR) spectra were recorded in the range of 800–2000 cm^{-1} with 4 cm^{-1} spectral resolution by using a Nicolet-IR100 FTIR spectrometer.

2.3. Electrochemical evaluation

The electrochemical activity of a prepared catalyst was evaluated in a three-electrode system using the CHI 1140A electrochemical workstation (from CH Instruments, Inc.) with a disk electrode as working electrode. The working electrode was prepared by loading 5 μL of catalyst ink onto a pretreated glassy carbon (GC) electrode (3 mm diameter and 0.07065 cm^2 geometrical area) and then dried at room temperature. Then, 8.0 mg of the catalyst sample, 3 mL ethanol, and 0.2 mL Nafion suspension (5 wt.%) were ultrasonically mixed to form a homogenous catalyst ink. Calomel electrode in saturated KCl solution (SCE) and Pt-wire electrodes were used as reference and counter electrodes, respectively. Cyclic voltammograms (CVs) of the electrodes were recorded between −1.0 and 0.2 V (vs. SCE) at 25 °C and a scan rate of 10 mV s^{-1} in an alkaline Ar or O_2-saturated solution (0.1 M KOH).

For powder catalyst evaluation, the use of the following approximate Koutechy–Levich (K–L) equation [20] is convenient for the estimation of the number of electrons transferred (n) per O_2 molecule through ORR:

$$j^{-1} = j_k^{-1} + \left\{0.62nFC_0D_0^{2/3}\nu^{-1/6}\omega^{1/2}\right\}^{-1} \quad (1)$$

where j_k is the kinetically apparent limiting current density, ω is the angular frequency of rotation, and F is the Faraday constant. The O_2 concentration (C_0), diffusion coefficient (D_0) of O_2 in 0.1 M KOH solution, and kinematic viscosity (ν) of the 0.1 M KOH solution were 1.15×10^{-3} M, 1.95×10^{-5} cm^2 s^{-1}, and 0.008977 cm^2 s^{-1}, respectively [23].

Rotating disk electrode (RDE) voltammograms were recorded between −0.85 and −0.15 V (vs. SCE) at a scan rate of 10 mV s^{-1} under rotation rates of 300, 400, 600, 800 and 1250 rpm in a 0.1 M KOH solution saturated with O_2 at 25 °C. To evaluate the effect of the interaction among Co, N, and C in the Co-doped PPy-modified BP2000 on ORR, the test catalysts were assumed to have similar electroactive surface areas.

3. Results and discussion

3.1. Morphology and structure studies

Pyrrole is a heterocyclic aromatic organic compound that has a five-membered ring with the formula C4H4NH. The NH proton in pyrrole is moderately acidic. Pyrrole is easily polymerized through the oxidation of the pyrrole monomer to form PPy. BP2000 (from

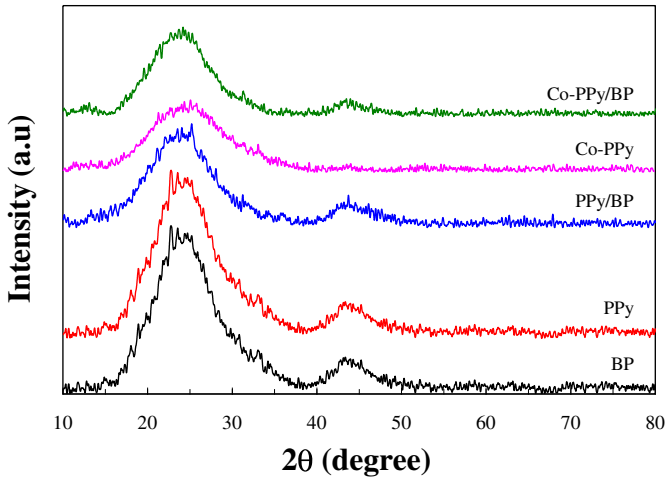

Fig. 1. XRD patterns of BP2000, PPy, PPy/BP, Co-doped PPy and Co-doped PPy/BP.

Cabot Corporation) is an amorphous carbon black used as electrocatalyst support. The wide XRD diffraction peaks of carbon at 26.1° and 44.2° indicate that BP2000 carbon and PPy have low crystallization degree, as shown in Fig. 1. No significant change in structure was observed through XRD identification after PPy-modification and hydrothermal Co-doping treatments (with Co nitrate as dopant), as shown in Fig. 2. No crystalline cobalt compound was detected using the XRD analyses.

Table 1
pH values of Co nitrate solutions before and after hydrothermal Co-doping treatment.

	BP (0.7 g)	PPy/BP (0.12 g/0.58 g)	PPy (0.7 g)
Co nitrate solution	5.52	5.52	5.52
After ultrasonic mixing	5.35	4.43	2.66
After hydrothermal treatment	4.89	4.14	1.80

Fig. 2a and b shows the morphologies of the purchased BP2000 and the synthesized PPy, respectively. PPy-modification and sequential hydrothermal Co-doping treatments changed the morphology of BP2000, as shown in Fig. 2c–e. PPy tied the carbon black particles together to form a 3D network during PPy modification. After hydrothermal Co-doping treatment, the PPy/BP particles were agglomerated to form a morphology similar to that of the Co-doped PPy sample. PPy reconfiguration occurred during the hydrothermal process, as shown in Fig. 2d and e. However, the reconfigured PPy preserved its non-crystalline characteristics, as shown in Fig. 1. Through pH measurement, the pH value of the $Co(NO_3)_2$ solution slightly decreased after ultrasonic mixing with PPy or PPy/BP, as shown in Table. 1. The pH value of the $Co(NO_3)_2$ solution further decreased in the sequential hydrothermal process. The pH value of the $Co(NO_3)_2$ solution decreased with increasing amounts of PPy in the sample, indicating that PPy reacted with Co^{2+} and released the NH proton of PPy during Co-doping, as suggested in the following reaction:

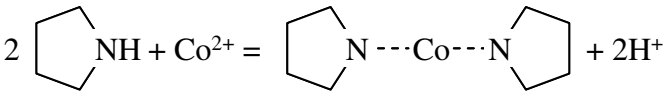

(2)

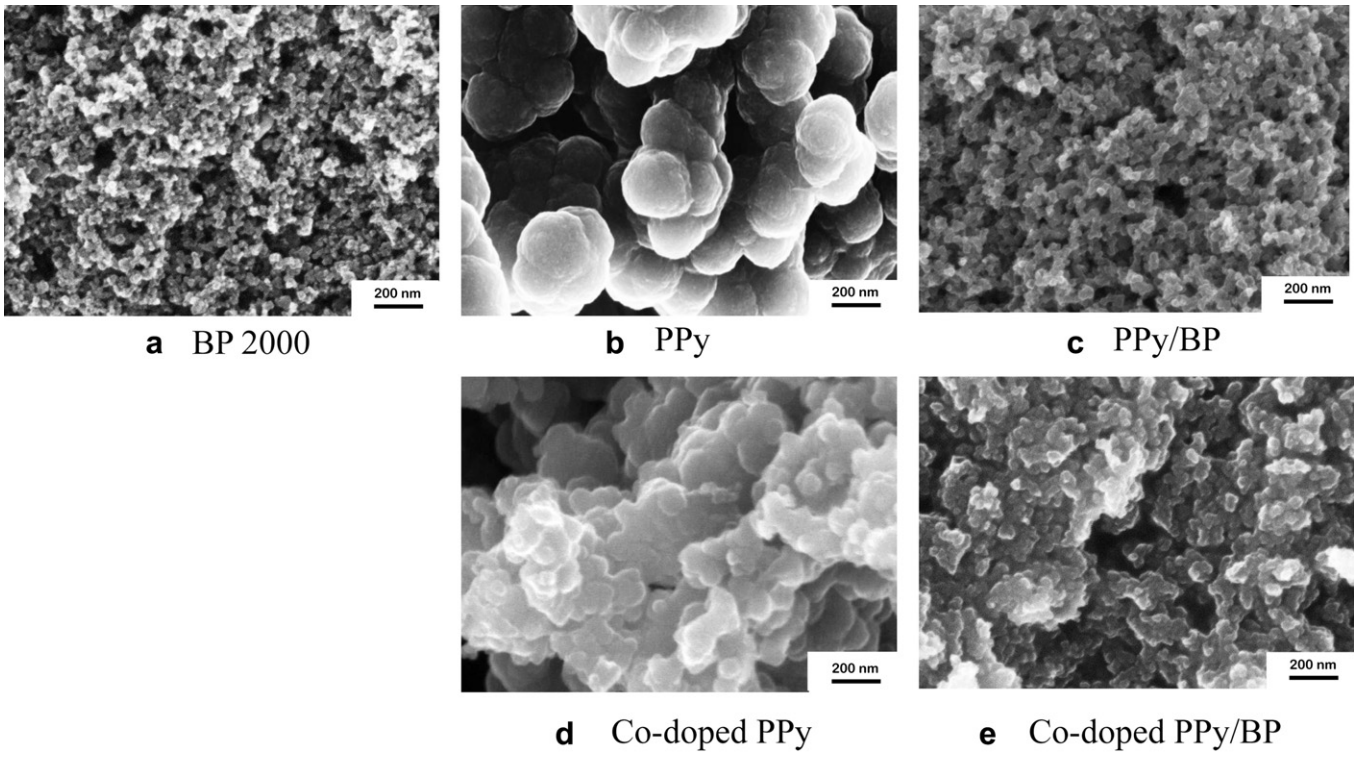

Fig. 2. Morphologies of (a) BP2000, (b) PPy, (c) PPy/BP, (d) Co-doped PPy and (e) Co-doped PPy/BP.

Table 2
Surface composition of BP2000 after PPy-modification and hydrothermal Co-doping treatment using Co nitrate as the dopant.

	C (at.%)	O (at.%)	N (at.%)	Co (at.%)
BP	90.8	9.2	–	–
PPy	76.9	12.3	10.8	–
PPy/BP	86.9	9.8	1.4	–
Co-doped PPy	75.6	16.1	8.1	0.2
Co-doped PPy/BP	88.0	10.3	1.5	0.2

According to the surface composition evaluation based on the results of the XPS analyses in Table. 2, the nitrogen-to-carbon ratio on the PPy surface (N:C ≈ 1:7) was found to be lower than that of PPy (N:C = 1:4), suggesting that the pyrrole ring was not parallel to the particle surfaces of PPy. Assuming that 10.8 at.% surface nitrogen content corresponds to a perfect PPy layer, the 1.4 at.% surface nitrogen content of PPy/BP indicates that only approximately 13% of the carbon surfaces was covered by PPy, as shown in the quantitative XPS analyses in Table. 2. Hydrothermal Co-doping treatment changed some of the surface nitrogen content.

3.2. XPS studies

Fig. 3 shows the normalized XPS spectra of the test samples based on the relative surface content of the constituents listed in Table. 2. According to the N1s core level spectra of PPy after spectral deconvolution [18–22], the 400.5, 399, and 398 eV binding energies were attributed to the "pyrrolic" nitrogen (–NH), "pyridinic" nitrogen (–C=N–C=), and Co–N bond, respectively. Pyrrolic-N is more electronegative than the nitrogen in the Co–N bond. Co-doping into PPy caused the binding energy of the N1s electron to shift to a lower energy of 398 eV, as shown in Fig. 3a, suggesting that the pyrrolic nitrogen in PPy broke its bond with hydrogen and created a bond with cobalt. This result coincides with the pH value changes in the Co nitrate solutions after the hydrothermal Co-doping treatment.

As can be seen in Table. 2 and Fig. 3d, only a small amount of Co was doped into PPy and PPy/BP, indicating that not all surface nitrogen can bind with Co. Some space factors may influence the formation of Co–N*x*. The Co-doping into PPy/BP exhibited a more significant binding energy shift than the Co-doping into PPy because of the abundance of Co–N bond in the Co-doped PPy/BP (Co:N = 1:7.5), which is more than that in the Co-doped PPy (Co:N = 1:40), relative to the Co and N contents on the surfaces.

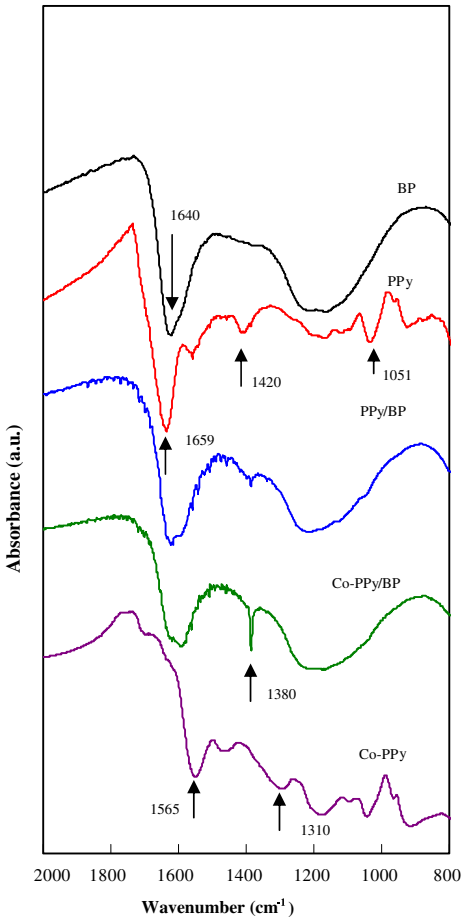

Fig. 4. FTIR spectra of BP2000, PPy, PPy-modified BP and Co-doped PPy/BP.

According to the O1*s* spectrum of PPy [18], the oxygen on the surface of PPy combined with carbon in the form of carbonyl (C=O 531.5 eV) and hydroxyl (C–OH at 533.2 eV). However, the oxygen on the surfaces of PPy/BP and the Co-doped PPy/BP bound carbon in the form of C–OH at 533.2 eV, similar to BP2000, because only approximately 13% of the carbon surfaces were covered by PPy.

PPy consists of SP^3 hybridized carbon (at 284.8 eV, α-position in the pyrrole molecular structure) and SP^2 hybridized carbon (at 283.84 eV, β-position) [18]. As an amorphous carbon [24,25],

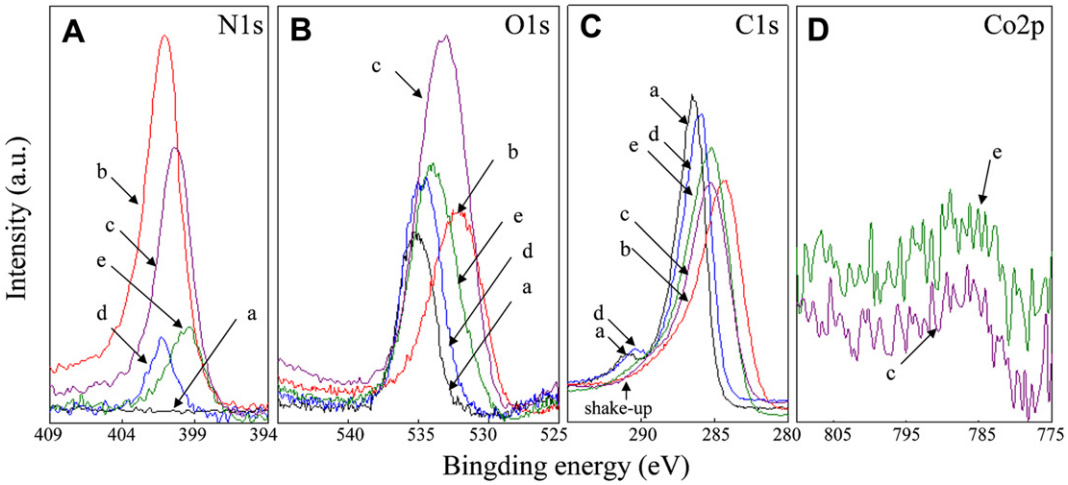

Fig. 3. Normalized X-ray photoemission spectra of (A) N1*s*, (B) O1*s*, (C) C1*s* and (D) Co2*p* for (a) BP2000, (b) PPy, (c) Co-doped PPy, (d) PPy/BP and (e) Co-doped PPy/BP, respectively.

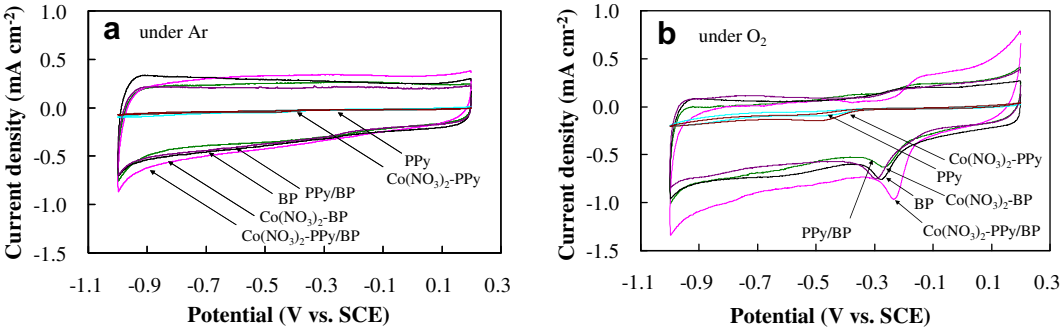

Fig. 5. CVs of BP, PPy, PPy/BP, Co-BP, Co-PPy and Co-PPy/BP in the alkaline (a) Ar- or (b) O_2-saturated solution (0.1 M KOH) at 25 °C. Scan rate: 10 mV s^{-1}.

BP2000 consists of SP^2 hybridized carbon (graphitic-C at 284.84 eV) and SP^3 hybridized carbon (diamond-like carbon at 285.8 eV). The binding energy of the C1*s* electron of the SP^2 hybridized carbon in BP2000 is similar to that of the α-position carbon of PPy. A shake-up appeared at approximately 291 eV in BP2000. This shake-up is only attributed to BP2000 because it did not appear in the C1*s* spectrum of PPy.

PPy modification on BP2000 caused the C1*s* peak of PPy/BP to shift to low binding energy but it indicated an insignificant affect on the shake-up, revealing that PPy modification did not affect BP2000 because the shift in C1*s* peak was caused by the increase in the α-position carbon of PPy. Therefore, active N-doped carbon cannot be formed through PPy modification on BP2000. However, Co-doping into PPy/BP causes not only a shift in its C1*s* peak to a lower binding energy but also the disappearance of the shake-up. Co establishes a certain relation with the carbon of BP2000 that reduces the SP^3 hybridized carbon portion on the carbon surfaces, whereas an increase in SP^2 carbon and a decrease in SP^3 carbon are important to enhance ORR [5]. These results show that the Co in the Co-doped PPy/BP acts not only on the nitrogen in PPy but also on the carbon in BP2000.

3.3. FTIR studies

XPS analyzes the kinetic energy and the number of electrons that escape from a certain element of the catalyst, whereas FTIR analysis focuses on the interaction among such elements. XPS analysis cannot distinguish the difference in C1*s* electron binding energy between C—C and C—N, but FTIR analysis can. According to FTIR studies on PPy [26–28], the characteristic absorption bands of polypyrrole can be observed at approximately 1659, 1565, and 1420 cm^{-1}, as shown in Fig. 4. The absorption peak at approximately 1659 cm^{-1} corresponds to the amines in the pyrrole structure (—NH) (pyrrolic-N, as described in XPS analysis). The bands at approximately 1565 and 1420 cm^{-1} correspond to the C—C and C—N stretching vibrations in the pyrrole ring, respectively. The characteristic absorption bands of the carbon materials were observed at approximately 1640 cm^{-1} (C=C stretching vibration). Significant differences in the FTIR spectra of BP2000, PPy, Co-doped PPy, and Co-doped PPy/BP were observed in the region of 1750–1200 cm^{-1}, which corresponds to the —NH, C—C, and C—N stretching vibrations in the pyrrole ring.

The FTIR spectrum of PPy/BP is similar to that of BP2000 because only 17 wt.% of PPy was loaded onto BP2000 and approximately 13% of the carbon surfaces were covered with PPy. Using hydrothermal Co-doping treatment, the —NH stretching vibration of the Co-doped PPy ceased, revealing that —NH disintegrated to form a new group. The XPS results indicate that the newly formed group is the bond of Co—N*x*. Correlated with the change in pH value of the Co nitrate solution during the hydrothermal Co-doping treatment, pyrrolic proton is known to release from —NH when the Co—N*x* group is formed after the hydrothermal Co-doping treatment.

Compared with the C—N stretching vibrations at approximately 1420 cm^{-1} in the pyrrole ring of PPy, the C—N stretching vibrations of the Co-doped PPy/BP shifted to lower frequency (red shift), revealing that pyrrolic-N was affected by Co-doping. The C—N stretching vibrations slowed down because of the drag of Co from Co—N*x*, further proving the existence of Co—N*x*. Notably, the C—N bonds in the Co-doped PPy were different compared with those in the Co-doped PPy/BP because the bands at approximately 1420 cm^{-1} (related to the C—N stretching vibrations) disappeared, suggesting that some of the C—N bonds in the Co-doped PPy/BP were different from those in the Co-doped PPy.

The bands at approximately 1051 cm^{-1} correspond to the =C—H in-plane vibration and N—H in-plane deformation [26]. The β-position (=C—H) is a stable position in the pyrrole ring during polymerization, and thus, the bands at approximately 1051 cm^{-1} can be recognized as the reference of the pyrrole ring. Therefore, Co-doping can change the characteristic absorption bands of PPy at

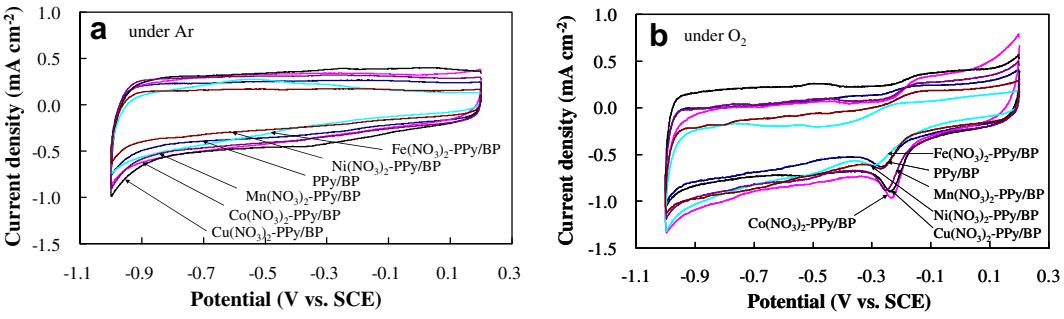

Fig. 6. CVs of M-doped PPy/BP (M = Mn, Fe, Co, Ni, Cu) in the alkaline (a) Ar- or (b) O_2-saturated solution (0.1 M KOH) at 25 °C. Scan rate: 10 mV s^{-1}.

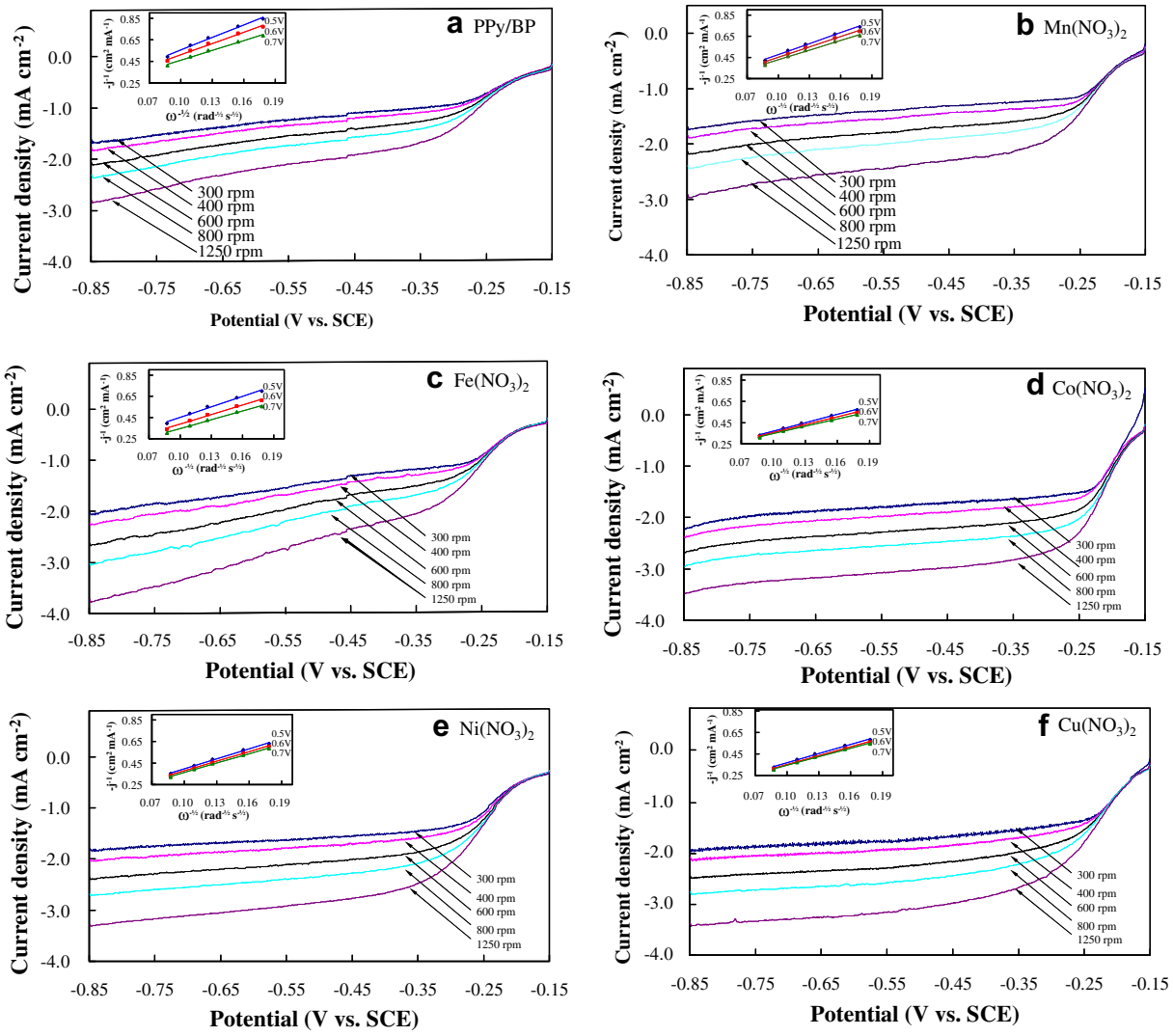

Fig. 7. RDE voltammograms and Koutechy–Levich (K–L) plots obtained from (a) non-doped PPy/BP, (b) Mn-doped PPy/BP, (c) Fe-doped PPy/BP, (d) Co-doped PPy/BP, (e) Ni-doped PPy/BP, (f) Cu-doped PPy/BP electrodes in the O_2-saturated KOH solution (0.1 M) at 25 °C. Scan rate: 10 mV s^{-1}. The inset shows K–L plots obtained at 0.5, 0.6, 0.7 V vs. SCE.

approximately 1659 cm^{-1} (α-position), but not at approximately 1051 cm^{-1} (β-position), as shown in Fig. 4.

3.4. Electrochemistry studies

BP2000 exhibited a certain ORR current but PPy did not, as shown in Fig. 5, revealing that the C sites on the BP particles catalyzed ORR but those on the PPy particles did not. PPy modification on BP2000 and Co-doping into BP2000 or PPy (with Co nitrate as dopant) exhibited insignificant effect on improving ORR kinetics, reflecting that the individual interactions between carbon support and PPy, carbon support and Co, and Co and PPy are not keys to the enhancement of the ORR process. However, Co-doping into PPy/BP improved ORR kinetics, as shown in Fig. 5b. The correlation of the XPS and FTIR results with the CV results revealed that doping Co to PPy can form Co–N*x*. However, Co–N*x* on PPy did not exhibit significant electroactivity to ORR, indicating that Co-doping is effective on PPy/BP but not on PPy relative to enhancement of ORR and revealing that the cooperative interaction (synergy) among Co, N (from PPy), and C (from BP2000) is the key towards improving ORR kinetics.

Studies on M-tetrasulfonated phthalocyanines [29] concluded that the doping effects on the electrocatalytic activity of ORR depend on the dopant elements because the bonds of M–N*x* affect the ORR pathways. Fig. 6 shows the CVs of M-doped PPy/BP catalysts in the Ar and O_2-saturated solutions. No significant anodic and cathodic peak current is observed in Fig. 6a (in the Ar-saturated solution). The significant cathodic currents in Fig. 6b represent that ORR occurred on the M-doped PPy/BP catalysts in the O_2-saturated solution. The small anodic currents appearing around −0.2 V reveal that something (only created in the O_2-saturated solution) electrochemically oxidized, indicating that the ORR on the M-doped PPy/BP catalysts is not a perfect four-electron-transfer reaction. Fig. 7 shows the RDE voltammograms and the K–L plots of the M-doped catalysts supported on the glass carbon

Table 3
Doping effects of transition elements on the number of electrons transferred (n) and kinetically apparent limiting current density (j_k).

	PPy/BP	$Mn(NO_3)_2$	$Fe(NO_3)_2$	$Co(NO_3)_2$	$Ni(NO_3)_2$	$Cu(NO_3)_2$
n	2.6	2.8	3.0	3.7	3.1	3.3
$-j_k$ (mA cm^{-2})	2.0	7.9	10.8	8.9	12.3	12.3

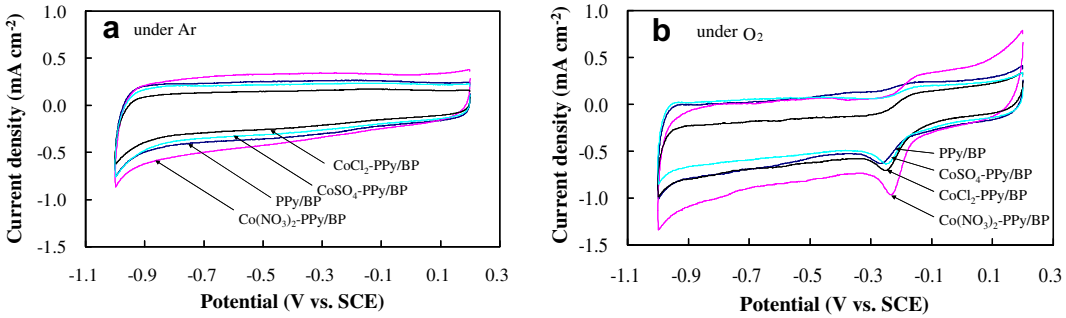

Fig. 8. CVs of Co-doped PPy/BP (using nitrate, chloride and sulfate as the precursor, respectively) in the alkaline (a) Ar- or (b) O_2-saturated solution (0.1 M KOH) at 25 °C. Scan rate: 10 mV s^{-1}.

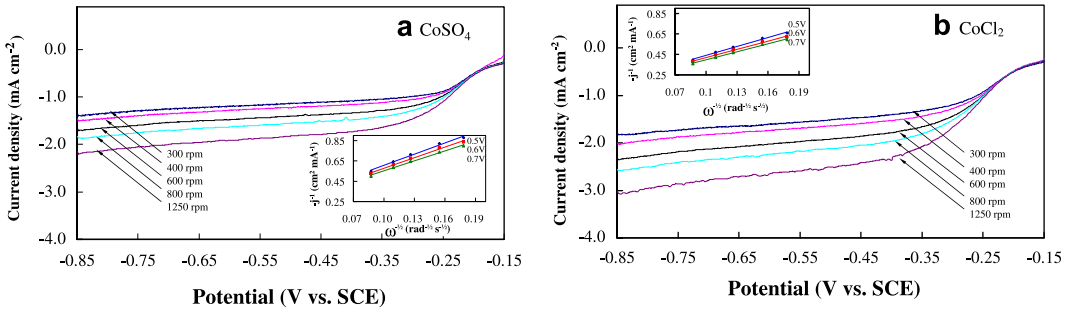

Fig. 9. RDE voltammograms and Koutechy–Levich (K–L) plots of Co-doped PPy/BP using (a) sulfate or (b) chloride as the precursor, respectively. The inset shows K–L plots obtained at 0.5, 0.6, 0.7 V vs. SCE at 25 °C.

electrode at 300, 400, 600, 800 and 1250 rpm rotation rates. The doping effects of such transition elements on the number of electrons transferred (n), as well as the kinetically apparent limiting current density (j_k), are illustrated in Table. 3, sorted according to their atomic number. Compared with hydrothermally treated PPy/BP, transition element doping promotes oxygen utilization (increase in n value) and improves electroactivity (increase in the absolute value of j_k). By increasing the d-electron of the transition element from 5 of Mn to 10 of Cu, the n value initially increased and then decreased, revealing that M–Nx with a proper empty d-orbit favors parallel coordination with one of two oxygen atoms and that another oxygen atom is then absorbed on the carbon atom (the edge carbon of the catalyst support, near the M–Nx site).

Pyridinic-N is a catalytic site for ORR through a two-eletron-transfer pathway [30]. PPy modification on BP2000 created pyridinic-N sites [20]. Hydrothermal treatment may create more catalytic sites, such as graphitic-N on PPy/BP, similar to N-doping with graphene through pyrolysis [31]. Consequently, the number of electrons transferred per molecular O_2 on the hydrothermally treated PPy/BP is promoted.

On the other hand, the doping anion plays an important role in improving the conductivity of PPy, as described in the study of doping anions in oxide/polypyrrole composites for ORR [32]. Fig. 8 shows the CVs of the Co-doped PPy/BP catalysts using nitrate, chloride or sulfate as the precursor. No significant anodic and cathodic peak current appears in the CVs of these catalysts in the Ar-saturated solution. Fig. 9 shows the RDE voltammograms and K–L plots of the Co-doped catalysts supported on the glass carbon electrode. Comparing Fig. 7d with Fig. 9a and b, Co nitrate exhibited a better doping effect than Co chloride or sulfate, revealing that anion-doping affects the ORR kinetics and pathway, as tabulated in Table. 4. When Co^{2+} ions combined with N of PPy to form M–Nx, the corresponding anions were then incorporated onto PPy to change the layered structures of the PPy backbone and the dopant [33]. This anion incorporation may change the electronic structure of graphitic-N to affect its electrocatalysis for ORR.

4. Catalytic sites for ORR on M-doped PPy-modified BP

The experimental results and discussion above show that hydrothermal M-doping into PPy/BP creates functional and non-functional M–Nx sites, as shown in Fig. 10. Functional M–Nx sites were formed near the graphite base (depending on the edge space of the graphite structure), enabling the molecular oxygen to be absorbed on carbon (from the catalyst support) and Co in bridge form. Consequently, ORR proceeds via the four-electron path on the M–Nx sites of carbon-supported catalysts [18–22]. The PPy in the Co-doped PPy released more NH protons than that in the PPy/BP (relative to the pH value), whereas the Co content on the surfaces of the Co-doped PPy and Co-doped PPy/BP were similar (from the XPS results), revealing that the Co in the Co-doped PPy combined more nitrogen than that in the Co-doped PPy/BP. Consequently, molecular oxygen will be difficult to absorb on Co. Therefore, without carbon support, hydrothermal M-doping into PPy only creates non-functional M–Nx sites.

Graphitic-N can be created from a graphitic ring through PPy reconfiguration during hydrothermal treatment, as shown in Fig. 10. Compared with M–Nx and graphitic-N, pyridinic-N formation is more difficult because of the geometrical limitation

Table 4
Effects of doping anions on the number of electrons transferred (n) and kinetically apparent limiting current density (j_k).

	PPy/BP	$CoSO_4$	CoC_{l2}	$Co(NO_3)_2$
n	2.6	2.6	3.4	3.7
$-j_k$ (mA cm^{-2})	2.0	4.3	6.9	8.9

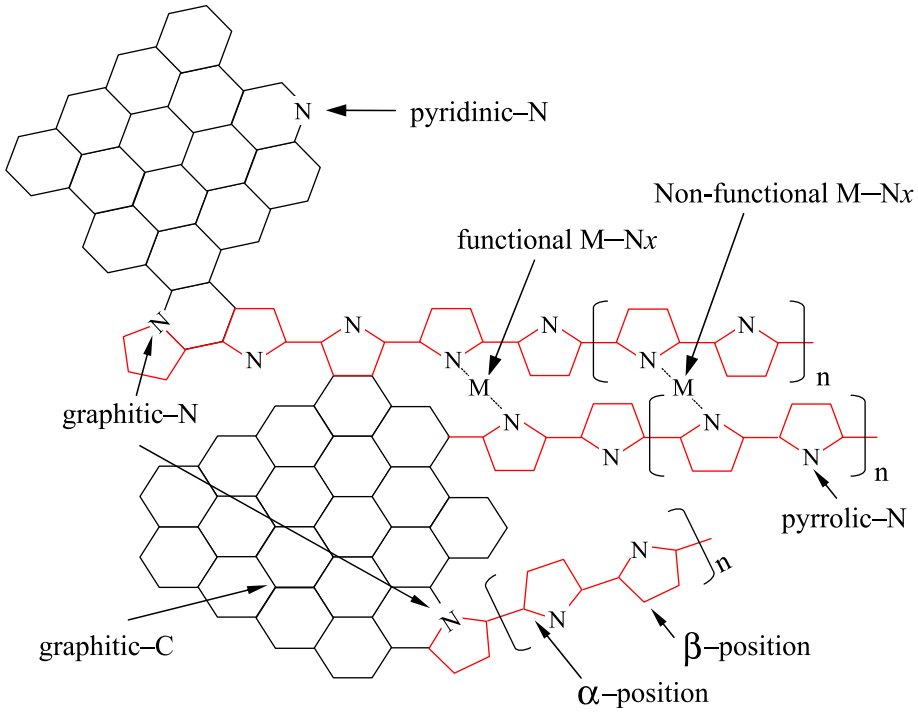

Fig. 10. Schematic representation of the catalytic sites on M-doped PPy/BP catalyst.

caused by the difference in molecular structure between graphite and pyrrole. Pyrolyzation may be necessary to create more pyridinic-N sites, as suggested by many researchers [6,7]. A surfactant containing Co may be a good catalyst precursor for treating PPy-modified carbon materials for ORR because Co-doping creates Co–N*x*. Moreover, the corresponding bulky anion can improve the electrical conductivity of PPy. PPy functions as an "electronic conductive wire" that connects each carbon particle to improve the conductivity of the catalyst.

5. Conclusions

M-doped PPy-modified BP2000 catalysts (M = Mn, Fe, Co, Ni, and Cu) were synthesized using the hydrothermal method. PPy ties carbon black particles together to form a 3D network after the PPy modification of BP2000. PPy reconfiguration occurs during the hydrothermal process. The cooperative interaction among Co, N (from PPy), and C (from BP2000) in the Co-doped PPy/BP is key to ORR enhancement as molecular oxygen is adsorbed on carbon (from catalyst support) and Co in bridge form. The individual interactions between carbon support and PPy, carbon support and Co, and Co and PPy exhibited insignificant effect on ORR enhancement. The doping effect of transition-metal salt to PPy/BP on ORR enhancement is dependent on the nature of the transition element and the corresponding anion.

Acknowledgments

The authors are grateful for the financial support received from the National Natural Science Foundation of China (Grant Nos. 20976156 and 50971114), the Zhejiang Provincial Natural Science Foundation of China (Grant No. Z4110126), the Doctoral Fund from the Education Ministry of China (20100101110042), and the Fundamental Research Funds for the Central Universities.

References

[1] P.A. Christensen, A. Hamnett, D. Linares-Moya, Physical Chemistry Chemical Physics 13 (2011) 5206–5214.
[2] C.F. Zinola, A.J. Arvia, G.L. Estiu, E.A. Castro, Journal of Physical Chemistry 98 (1994) 7566–7576.
[3] J.A. Menendez, J. Phillips, B. Xia, L.R. Radovic, Langmuir 12 (1996) 4404–4410.
[4] H. Jin, H. Zhang, H. Zhong, J. Zhang, Energy & Environmental Science 4 (2011) 3389–3394.
[5] H. Niwa, M. Kobayashi, K. Horiba, Y. Harada, M. Oshima, K. Terakura, T. Ikeda, Y. Koshigoe, J. Ozaki, S. Miyata, S. Ueda, Y. Yamashita, H. Yoshikawa, K. Kobayashi, Journal of Power Sources 196 (2011) 1006–1011.
[6] H. Oh, J. Oh, W.H. Lee, H. Kim, H. Kim, International Journal of Hydrogen Energy 36 (2011) 8181–8186.
[7] V.V. Strelko, N.T. Kartel, I.N. Dukhno, V.S. Kuts, R.B. Clarkson, B.M. Odintsov, Surface Science 548 (2004) 281–290.
[8] S. Maldonado, K.J. Stevenson, Journal of Physical Chemistry B 109 (2005) 4707–4716.
[9] J.S. Spendelow, A. Wieckowski, Physical Chemistry Chemical Physics 9 (2007) 2654–2675.
[10] F.H.B. Lima, J.F.R. de Castro, E.A. Ticianelli, Journal of Power Sources 161 (2006) 806–812.
[11] Z.P. Li, B.H. Liu, Journal of Applied Electrochemistry 40 (2010) 475–483.
[12] L. Zhang, K. Lee, C.W.B. Bezerra, J. Zhang, J. Zhang, Electrochimica Acta 54 (2009) 6631–6636.
[13] M. Lefevre, E. Proietti, F. Jaouen, J.P. Dodelet, Science 324 (2009) 71–74.
[14] R. Bashyam, P. Zelenay, Nature 443 (2006) 63–66.
[15] H.Y. Qin, Z.X. Liu, S.J. Lao, J.K. Zhu, Z.P. Li, Journal of Power Sources 195 (2010) 3124–3129.
[16] H.Y. Qin, Z.X. Liu, W.X. Yin, J.K. Zhu, Z.P. Li, Journal of Power Sources 185 (2008) 909–912.
[17] H.Y. Qin, Z.X. Liu, L.Q. Ye, J.K. Zhu, Z.P. Li, Journal of Power Sources 192 (2009) 385–390.
[18] C. Malitesta, I. Losito, L. Sabbatini, P.G. Zambonin, The Journal of Electron Spectroscopy and Related Phenomena 76 (1995) 629–634.
[19] V. Nallathambi, J.W. Lee, S.P. Kumaraguru, G. Wu, B.N. Popov, Journal of Power Sources 183 (2008) 34–42.
[20] H.Y. Qin, K.N. Zhu, L.Q. Ye, Z.P. Li, Journal of Power Sources 208 (2012) 203–209.
[21] C.Z. Deng, M.J. Dignam, Journal of Electrochemical Society 145 (1998) 3507–3512.
[22] G. Wu, M.A. Nelson, N.H. Mack, S.G. Ma, P. Sekhar, F.H. Garzon, P. Zelenay, Chemical Communications 46 (2010) 7489–7491.
[23] D. Zhang, D. Chi, T. Okajima, T. Ohsaka, Electrochimica Acta 52 (2007) 5400–5406.
[24] S.T. Jackson, R.G. Nuzzo, Applied Surface Sciences 90 (1995) 195–203.

[25] R. Haerle, E. Riedo, A. Pasquarello, A. Baldereschi, Physical Review B 65 (2001) 045101.
[26] A. Mollahosseini, E. Noroozian, Synthetic Metals 159 (2009) 1247–1254.
[27] J. Liu, M. Wan, Journal of Material Chemisty 11 (2001) 404–407.
[28] J.V. Koleske (Ed.), Paint and Coating Testing Manual: Fourteenth Edition of the Gardner-Sward Handbook, ASTM Pub, 1995 (Chapter 44) p. 517.
[29] J.H. Zagal, Coordination Chemistry Reviews 119 (1992) 89–136.
[30] Z. Luo, S. Lim, Z. Tian, J. Shang, L. Lai, B. MacDonald, C. Fu, Z. Shen, T. Yu, J. Lin, Journal of Material Chemistry 21 (2011) 8038–8044.
[31] Z. Lin, M. Song, Y. Ding, Y. Liu, M. Liu, C. Wong, Physical Chemistry Chemical Physics 14 (2012) 3381–3387.
[32] H.N. Cong, K.E. Abbassi, J.L. Gautier, P. Chartier, Electrochimica Acta 50 (2005) 1369–1376.
[33] G.R. Mitchell, F.J. Davis, C.H. Legge, Synthetic Metals 26 (1988) 247–257.